Nano and Medical Materials 2023, 3(1), 73.
https://doi.org/10.59400/nmm.v3i1.73

Article

Biofabricated MoO_3 nanoparticles for biomedical applications: Antibacterial efficacy, hemocompatibility, and wound healing properties

Anisha Salim[1], Subramaniam Sadhasivam[1,2,*]

[1] Department of Microbial Biotechnology, Bharathiar University, Coimbatore 641046, India
[2] Centre for International Affairs, Bharathiar University, Coimbatore 641046, India
*** Corresponding author:** Subramaniam Sadhasivam, sadhaofficial@buc.edu.in

CITATION

Salim A, Sadhasivam S. Biofabricated MoO3 nanoparticles for biomedical applications: Antibacterial efficacy, hemocompatibility, and wound healing properties. Nano and Medical Materials. 2023; 3(1): 73. https://doi.org/10.59400/nmm.v3i1.73

ARTICLE INFO

Received: 14 June 2023
Accepted: 31 July 2023
Available online: 9 August 2023

Abstract: This study presents a simple, eco-friendly, and cost-effective method for synthesizing molybdenum trioxide nanoparticles (MoO_3 NPs) using the medicinal plant *Hemigraphis alternata*. The physicochemical characterization confirmed the formation of orthorhombic MoO_3 NPs. The green synthesized NPs exhibited remarkable antioxidant and antimicrobial properties against multi drug-resistant bacteria (*S. aureus* and *P. aeruginosa*) and fungi (*A. niger* and *C. albicans*) in a concentration-dependent manner. Hemocompatibility assessments on human erythrocytes suggested their potential application in wound healing. Cytotoxicity evaluations on mouse fibroblast cell lines demonstrated no harmful effects. Furthermore, in vitro scratch assays revealed over 90% wound healing activity without cytotoxicity. The findings indicate that these green synthesized MoO_3 NPs hold promise for incorporation into wound dressings, offering a safe and effective solution for infectious wound healing. This study represents a novel effort to update practitioners on the latest developments in the widespread use of green synthesized NPs in medicine.

Keywords: green synthesis; MoO_3 NPs; hemocompatability; cytotoxicity; antimicrobial; wound healing activity

1. Introduction

In the field of contemporary materials science, nanotechnology has ushered in significant advancements in the development of diagnostic and therapeutic nanomedicine [1]. Nanotechnology revolves around the manipulation and utilization of metals and metal oxides at the nanoscale, harnessing their unique size, surface characteristics, and physicochemical properties [2,3]. Notably, nanotechnology has found widespread use in skincare, where metal and metal oxide nanoparticles (NPs) such as titanium dioxide and zinc oxide are incorporated into cosmetics to provide effective sun protection [4]. Inorganic nanostructures have garnered considerable attention for their potential applications in creating innovative functional materials for biological purposes [5]. Extensive research has explored various chemical and physical methods for synthesizing metal and metal oxide nanoparticles [6]. However, concerns have been raised regarding potential toxicity associated with chemical synthesis methods, which could pose risks in biological environments. As a result, plant based approaches for producing metallic nanoparticles have gained significance due to the presence of diverse biomolecules, including vitamins, proteins, surfactants, and carbohydrates derived from plant extracts [2,7,8].

Plant extracts are known for their high antioxidant activity and reducing capacity, which enables them to effectively reduce metal salts into metallic nanoparticles [1]. Several studies have been conducted to investigate the

antibacterial characteristics of various metal nanoparticles, including Ag, Cu, and Au, as well as metal oxide nanoparticles such as ZnO, MgO, and CuO [3,9–11]. Molybdenum trioxide (MoO_3) has recently gained attention as a bio-functional substance with antibacterial and anticancer properties. Additionally, MoO_3 finds wide application in energy storage, photocatalysis, and sensor-related fields [12]. In mammals, molybdenum (Mo) serves as an essential trace metal, acting as a cofactor for enzymes such as sulfite oxidase and xanthine oxidase. Mo deficiency in patients undergoing prolonged total parenteral nutrition can lead to clinical symptoms like coma, tachycardia, tachypnea, and night blindness [13]. Molybdenum complexes have also demonstrated antidiabetic activity, and the permitted daily intake of Mo is 2 mg [14]. MoO_3 nanoparticles (MoO_3 NPs) exhibit the lowest level of toxicity among NPs used in medicine, and they induce an acidic pH while demonstrating broad-spectrum antibacterial activity against both susceptible and resistant strains of bacteria, including those responsible for hospital-acquired infections [15,16]. Their potent antibacterial and pro-angiogenic activities make MoO_3 NPs particularly suitable for wound healing applications [15]. While silver nanoparticles have been extensively studied for their broad-spectrum antibiotic capabilities, their high cost and release of toxic silver ions limit their applications. In contrast, MoO_3 NPs offer a promising alternative due to their antibacterial mechanism, which involves inducing membrane or oxidative stress, leading to the rupture of bacterial cell walls and subsequent cell death [3]. Compatibility studies in a rat liver-derived cell line (BRL 3A) have shown that MoO_3 NPs exhibit higher compatibility compared to silver NPs [17]. However, it's worth noting that MoO_3 NPs do exhibit significant cytotoxicity against both lung and breast cancer cells, as well as potent antifungal activity against *Candida albicans* and *Aspergillus niger* [18].

The Acanthaceae family includes the medicinal plant *Hemigraphis alternata* (HA) (Burm.F.) T. Anderson, commonly known as Red Ivy or Purple Waffle Plant and locally called Murikootti (Malayalam) [19,20]. HA has gained recognition among tribal healers in southern India for its potential in wound treatment [21]. The plant has been traditionally used in folk medicine to treat various conditions, including anaemia, fresh wounds, ulcers, gallstones, diuretics, haemorrhoids, diabetes mellitus, and inflammation. HA extract has been studied for its therapeutic benefits and has been found to contain various bioactive compounds such as flavonoids, glucose, carboxylic acids, saponins, and other phenolic derivatives [20,22]. Notably, cinnamate, a significant phenolic acid found in Hemigraphis, possesses potent antibacterial properties. The crude leaf extract of HA has been shown to be effective in treating inflammation, and when combined with chitosan hydrogel, it exhibits synergistic effects against gram-positive and gram-negative bacteria [23]. Furthermore, studies have validated the anti-inflammatory, antinociceptive, and antidiarrheal effects of methanol and ethyl acetate extracts of HA leaves in mice [24]. Additionally, the aqueous and organic extracts of HA have been shown to facilitate wound exudate absorption, help maintain a low body temperature, and possess antinociceptive effects [25].

The primary objective of this study is to synthesize MoO_3 NPs using extracts from HA leaves and investigate their antimicrobial activity against a range of human pathogens. The synthesized NPs were thoroughly characterized using various

analytical methods, and their antioxidant, antimicrobial, and hemocompatibility properties were evaluated. Additionally, the wound healing potential of the MoO_3 NPs was assessed using L929 mouse fibroblast cell lines. The research findings from this study will contribute valuable insights into the potential biomedical applications of MoO_3 NPs derived from HA leaves.

2. Materials and methods

2.1. Materials

All the reagents used in this experiment were of analytical grade and were used without any additional purification. The metal precursor salts were obtained from Sigma Aldrich (India). The plant extract was obtained from *Hemigraphis alternata* leaves. Distilled water was used throughout the experiment.

2.2. Collection and investigation of *Hemigraphis alternata* plant

Healthy and disease-free fresh leaves of *Strobilanthes alternata* were collected during their blooming stage from Trippalur, Palakkad, India. The plant specimen was identified as *Strobilanthes alternata* (Burm.F.) Moylan ex J.R.I.Wood (Syn.: *Hemigraphis alternata* (Burm.F.) T.Anderson) from the Acanthaceae family, and its authenticity was confirmed with the herbarium number BSI/SRC/5/23/2023-24/Tech-310 at the Botanical Survey of India (BSI), Southern Regional Centre, Coimbatore. To prepare the leaves for further use, they were thoroughly cleaned. Initially, the leaves were rinsed with tap water to remove any visible dirt or impurities. Then, they were washed with detergent water to eliminate any remaining contaminants. Finally, the leaves were rinsed again with distilled water to remove any residual foreign matter. Subsequently, the cleaned leaves were allowed to dry for a week, further powdered and then carefully sealed for future experiment.

2.3. Green synthesis of MoO_3 NPs

Fresh aqueous leaf extracts of *Hemigraphis alternata* were used in the bio-approach for the synthesis of MoO_3 NPs [26]. Ammonium heptamolybdate (0.1 mM) was dissolved in 100 mL of distilled water and allowed to dissolve for 30 min. Under constant stirring, the filtered *Hemigraphis alternata* leaf extract was slowly added drop by drop to the homogenous solution of ammonium heptamolybdate. The solution was heated at 70 °C while continuously stirring until the supernatant evaporated. This led to the formation of a dry residue, which had a brown color. The dry residue obtained from the previous step was subjected to calcination in a muffle furnace. The temperature increased by 5 °C every minute over the 2 h of calcination, reaching a maximum temperature of 700 °C. The product's colour progressively changed from brown to silver grey during the calcination process. After calcination, the green synthesized MoO_3 NPs were finely crushed and stored in airtight containers for future experiment.

3. Characterization of MoO_3 NPs

3.1. UV spectroscopy

The MoO_3 NPs were initially analyzed using a UV-Vis spectrophotometer (Shimadzu-UV-2700 ISR-2600 plus) to measure their absorbance at various wavelengths in the range of 200 nm–1200 nm. This analysis provides information about the optical properties of the synthesized nanoparticles.

3.2. FTIR spectroscopy

FTIR study was conducted to analyze the functional groups and chemical bonds of the synthesized MoO_3 NPs. The FTIR analysis was performed using an FT/IR-4700 type A instrument, with measurements taken in the range of 4000–500 cm^{-1} at a resolution of 4 cm^{-1}.

3.3. XRD

The crystallite structure and size of the MoO_3 NPs were analyzed using a CuKα1-X-ray diffractometer (P-XRD) [Empyrean, Malvern Panalytical]. The X-ray diffraction measurements were performed over a 2θ range of 5°–90°. This investigation reveals details of the nanoparticles' crystal structure and enables estimation of their size from the observed diffraction patterns.

3.4. FESEM with EDAX

To visualize the size and morphology of the MoO_3 NPs, field emission scanning electron microscopy (FESEM) techniques were employed. Energy dispersive spectroscopy (EDAX) (accelerating voltage ranging from 0.5 kV to 30 kV) was used to confirm the elemental composition of synthesized materials. This imaging technique provides high-resolution images of the nanoparticles, allowing for the characterization of their shape, size, and surface morphology.

3.5. Dynamic light scattering (DLS) and zeta potential (ZP)

The DLS system was used to measure the hydrodynamic diameters of the NPs under examination. ZP calculates the net electrostatic potential of any particle in suspension and is the key component in assessing the stability of the synthesized NPs. The hydrodynamic diameter, ZP and polydispersity index (PDI) of the MoO_3 NPs was measured at 25 °C using Litesizer 500 (Ver. 2.30.4, Serial Number: 84045171).

3.6. Thermogravimetric analysis (TGA)

A TGA instrument (NETZSCH STA 449F3) was used to examine the thermal characteristics of the MoO_3 NPs. The sample was subjected to TGA and DTG at temperatures ranging from 30 to 800 °C in a dynamic nitrogen environment. The thermogravimetric curves were recorded using a TGA analysis with a heating rate of 10 °C/min. This analysis provides information about the thermal stability, decomposition behavior, and weight loss of the MoO_3 NPs with respect to temperature.

3.7. Antioxidant activity

The antioxidant compounds are naturally known to accelerate the healing process which reduces the oxidative stress caused by the radicals within the wounds. Metal oxide nanoparticles have the potential to act as scavengers of oxidative stress. The total antioxidant capacity of natural matrices is assessed using various standardized tests [27]. One commonly used test involves the stable free radical DPPH (2,2-diphenyl-1-picrylhydrazyl) to study the antioxidant capacity for scavenging radicals. In this study, MoO_3 NPs were tested for their ability to scavenge DPPH and ABTS (2,2'-azino-bis(3-ethylbenzothiazoline-6-sulfonic acid)) free radicals, following the technique researched by Rajkumar et al. with minor modifications [28]. A 0.5 mL volume of 1.5 mM DPPH solution was mixed with concentrations (ranging from 0.5 to 2 mg/mL) of MoO_3 NPs. The mixed solution was incubated under dark conditions for 30 min. After incubation, a UV spectrophotometer set to a wavelength of 517 nm was used to measure the absorbance. Similarly, for ABTS assay, different concentrations of MoO_3 NPs (0.5 to 2 mg/mL) were mixed with the prepared $ABTS^+$ solution (135 µL) and incubated for 30 min under dark conditions. With reference to the ascorbic acid as positive control, the absorbance of the samples was measured at a wavelength of 734 nm. The means and standard deviations were computed after each determination was made in triplicate.

The radical scavenging potential of the samples were evaluated using the below calculations:

$$\text{DPPH } or\ ABTS\ scavenging\ \% = [(Abs_{control} - Abs_{NPs})/Abs_{control}] \times 100$$

where $Abs_{control}$ and Abs_{NPs} is the absorbance of the control and treatment value.

3.8. Antimicrobial activity

3.8.1. Microbial culture

The clinical isolates of bacteria used in the study were obtained from PSG hospital in Coimbatore, India. According to the standards established by the Centers for Disease Control and Prevention/National Healthcare Safety Network (CDC/NHSN), these bacterial strains were isolated from clinical specimens of hospitalized patients. Methicillin-resistant Staphylococcus aureus (MRSA), a gram-positive bacterium, and *Pseudomonas aeruginosa*, a gram-negative bacterium are the two clinically important human bacterial pathogens. These strains are known for their resistance to multiple antibiotics and are of particular concern in healthcare settings.

In addition to the bacterial strains, two fungal strains, *Aspergillus niger* and *Candida albicans*, were used in the study. These fungal strains were procured from the Department of Microbial Biotechnology at Bharathiar University in Coimbatore. Fungal pathogens, such as *Aspergillus niger* and *Candida albicans*, are known to cause various infections, particularly in immunocompromised individuals. The use of clinically relevant bacterial and fungal strains ensures that the antimicrobial effects of the synthesized MoO_3 NPs can be evaluated against pathogens commonly encountered in health care settings.

3.8.2. Minimum inhibitory concentration (MIC)

MIC testing was performed on the green synthesized MoO_3 NPs against multi-drug resistant *S. aureus* and *P. aeruginosa.* The MIC of the MoO_3 NPs was measured using a serial dilution method, reported by Mogana et al. [29]. By dissolving the sample in water and bringing the concentration to a final volume of 200 µg/mL, stock solutions of the MoO_3 NPs were obtained. Serial dilutions of the MoO_3 NPs were prepared from the stock solution. These dilutions were made using Mueller-Hinton broth in 96-well microplates. A bacterial suspension containing approximately 5×10^5 CFU/mL was prepared from a 24 h culture plate of the respective bacteria. From this bacterial suspension, 100 µL was inoculated into each well of the microplate containing the dilutions of the MoO_3 NPs. The microplates were then incubated at 37 °C for a specified period of time. After incubation, the MIC values were determined. The MIC is characterized as the lowest concentration of MoO_3 NPs at which no discernible bacterial growth is detected. MIC values were determined in triplicate to ensure the reliability of the results. By assessing the MIC values, the minimum inhibitory concentration of the MoO_3 NPs against multi-drug resistant *S. aureus* and *P. aeruginosa* can be determined, indicating the effectiveness of the NPs in inhibiting bacterial growth.

3.8.3. Antibacterial activity

The antibacterial activity of the MoO_3 NPs against multi-drug resistant *S. aureus* and *P. aeruginosa* was determined using the well diffusion method [30]. Cultures of the bacteria (*S. aureus* and *P. aeruginosa*) were inoculated into nutrient broth and incubated for 24 h to allow bacterial growth at 37 °C. The bacterial suspension was then adjusted to match the McFarland standards, ensuring a standardized concentration of bacteria for testing. A volume of 0.1 mL of the bacterial cultures was spread evenly onto the surface of the agar plates. Using a sterile hole puncher, small wells were created in the agar plates. The MoO_3 NPs were added into each well, and the NPs seeded agar plates were incubated overnight. After 24 h of incubation, the zone of clearance around the well was measured to determine the antibacterial activity. The results were compared with a positive control, such as Cefmetazole, which is a known antibiotic. By measuring the inhibition zone, the antibacterial sensitivity of the MoO_3 NPs against multi-drug resistant *S. aureus* and *P. aeruginosa* can be determined and compared to the positive control.

3.8.4. Antifungal activity

The antifungal activity of the MoO_3 NPs against *A. niger* and *C. albicans* was assessed by the agar well diffusion method [31]. Fungal cultures of *A. niger* and *C. albicans* were allowed to grow on potato dextrose medium. Aliquots of 0.02 mL of the fungal inoculum were transferred into 20 mL of the culture medium in individual culture tubes. The culture tubes were homogenized to ensure even distribution of the fungal pathogens in the medium. Homogeneous wells were created in the agar plates using a sterile hole puncture and the different concentrations of the MoO_3 NPs (0.125, 0.25, 0.5, and 1 mg/mL) were added to the respective wells. The petri dishes were incubated for 48 h at 25 °C, allowing the fungal pathogens to grow and potentially be inhibited by the nanoparticles. After the incubation period, the growth inhibition zones around the wells were evaluated. The size of the inhibition zone

indicates the antifungal activity of the MoO_3 NPs against *A. niger* and *C. albicans*. By measuring the growth inhibition zones, the antifungal activity of the MoO_3 NPs against *A. niger* and *C. albicans* can be determined. The antifungal activity of the NPs increases with the size of the inhibitory zone.

3.8.5. Time-dynamic antibacterial assay

The antibacterial activity of MoO_3 NPs over time was evaluated by a time dynamic antibacterial assay [32]. Bacterial pathogens, such as *S. aureus* and *P. aeruginosa*, were prepared at a concentration of 10^7 CFU/mL. The bacterial cultures were divided into 2 groups: one group was treated with MoO_3 NPs, whereas group without nanoparticle served as the control. At regular intervals (every half hour) from 0 h to 4 h, samples of the bacterial cultures were collected. The collected samples were diluted in a gradient to obtain appropriate dilutions. Each dilution was then cultured on Luria-Bertani (LB) agar medium and subjected to incubation for 24 h at 37 °C. After the incubation, the number of bacterial colonies was estimated. By measuring the reduction ratio of bacterial colonies over time, the antibacterial activity of the MoO_3 NPs can be assessed. A higher reduction ratio indicates a greater antibacterial effect of the nanoparticles against *S. aureus* and *P. aeruginosa*. Each experiment was performed in triplicate for the reliability of results. The reduction ratio of bacterial colonies was calculated by the following equation:

$$\text{Reduction } ratio\ \% = [Ac - As/Ac] \times 100$$

where, *Ac* and *As* indicates the number of colonies in the control group and MoO_3 NPs treated group.

3.8.6. Assessment of protein leakage and reducing sugar

The ability of MoO_3 NPs to induce the leakage of biomolecules like protein and reducing sugar from the bacterial cell due to the disruption of cell wall was studied by the method described by Li et al. [33]. Bacterial pathogens, such as *S. aureus* and *P. aeruginosa*, were prepared at a concentration of 10^7 CFU/mL. The bacterial cultures were divided into 2 groups: one group was treated with MoO_3 NPs, whereas group without nanoparticle served as the control. Both the treated and control groups were incubated in shaker incubator at 37 °C for 4 h. After the incubation period, 1 mL of the bacterial aliquots was collected from all the samples and centrifuged at 12,000 rpm for 30 min to separate the supernatant from the bacterial cells. The concentration of leaked proteins and reducing sugars in the supernatant was measured and quantified, represented as μg/mL. By measuring the total leakage of biomolecules from the bacterial cells, the impact of MoO_3 NPs on the integrity of the cell membrane can be assessed. Higher levels of biomolecule leakage indicate a greater disruption of the cell membrane by the nanoparticles.

3.9. Hemolysis assay

The hemocompatibility of MoO_3 NPs was assessed using a hemolysis assay [34]. Briefly, the erythrocytes or the RBCs, were separated by centrifuging the blood at 1200 rpm at RT for 10 min. The serum was carefully separated from the suspension and the pelleted cells were suspended in a 100 mM sodium phosphate buffer (pH 7.4). Various concentrations of MoO_3 NPs (25, 50, 75, and 100 μg/mL)

were mixed with the RBC suspension. The reaction mixture was made up to the final volume of 1 mL by adding extra sodium phosphate buffer. Further, the mixture was kept in a water bath at 37 °C for a period of 1 h and subjected to centrifugation at 2500 rpm for 15 min. The supernatant containing released hemoglobin was collected and the optical density was measured at 541 nm by a spectrophotometer. Phosphate-buffered saline (PBS) served as positive control (maximum hemolysis). The hemolysis assay was performed in triplicate for each concentration of MoO_3 NPs.

The hemolytic activity of MoO_3 NPs was calculated using the following equation:

Hemolysis % = (Absorbance of MoO_3 NPs-Absorbance of blank) × 100/Absorbance of positive control

3.10. Cytotoxicity analysis

3.10.1. Maintenance of cell line

From the National Centre for Cell Science (NCCS) in Pune, the L929 mouse fibroblast cell line was obtained. Following standard cell culture procedures, the cells were grown and maintained in a humidified incubator (5% CO_2) at 37 °C.

3.10.2. MTT assay

The cytotoxicity of MoO_3 NPs was assessed using the 3-(4, 5-dimethyl-2-thiazolyl)-2,5-diphenyl-2H-tetrazolium bromide (MTT) assay [35]. In this assay, L929 cells were seeded in 96-well plates at a density of 3.0×10^3 cells per well in culture medium containing 10% fetal bovine serum (FBS) and 1% antibiotic solution. After incubating for 24 h, the wells were washed with sterile PBS and exposed to various concentrations (25, 50, 75, 100 µg/µL) of MoO_3 NPs. The cells were then incubated at 37 °C for 24 h. Control wells without MoO_3 NPs were included. After incubation, the supernatant medium was removed and replaced with 200 µL of dimethyl sulfoxide (DMSO). The absorbance of the formazan product was measured at 570 nm by a microplate reader. The experiment was performed in triplicate and cell viability (%) was calculated using the following formula:

$$\text{Cells } viability\,\% = (Abstreated\ cells/Abscontrol\ cells) \times 100$$

3.10.3. Scratch assay

The wound healing efficacy of MoO_3 NPs was evaluated using an in vitro scratch assay on L929 cells [36]. Initially, each well of a cell culture plate was seeded with 2×10^4 cells and incubated at 37 °C and 5% CO_2 for 24 h to allow the cells to reach 90% confluence. Once the cell monolayer was formed, a straight scratch was created using a sterile pipette tip. The debris was removed by washing the cells with PBS, and then the cells were treated with different concentrations of MoO_3 NPs (25 and 50 µg/µL) for 24 h. The proliferation of cells was monitored using an inverted phase-contrast microscope, and images of the scratch area were captured at 0 h, 12 h, and 24 h. The changes in the wound area over time were analyzed to assess the wound healing potential of MoO_3 NPs.

3.11. Statistical analysis

All the experiments were performed in triplicates, mean value for three replications and standard error (SE) were calculated. One-way ANOVA was used for the statistical analysis with SPSS version 12.0 (SPSS, Inc., Chicago, IL). When the *P* value was less than 0.05, the differences between experimental groups were deemed as significant.

4. Results and discussion

4.1. Visual observation and UV spectroscopy

The formation of MoO_3 NPs was determined by observing a change in color and using UV spectroscopy. Upon the addition of ammonium heptamolybdate to the plant extract, the reaction color transitioned from purple to brown, indicating the formation of MoO_3 NPs are given in **Figure 1a**. The absorption spectra of the green synthesized MoO_3 NPs were analyzed using UV spectrophotometry, are shown in **Figure 1b**. The maximum absorbance peak was observed at 257 nm in the UV-C region, which confirms that the aqueous extract of HA reduced Mo ions and facilitated the synthesis of MoO_3 NPs. Nanoparticles with dimensions ranging from 1 nm to 100 nm possess unique properties attributed to their high surface area and small size [37,38]. Kanneganti et al. [26] also synthesized MoO_3 NPs using citrus limetta pith extract, and their study exhibited a characteristic peak at 257 nm.

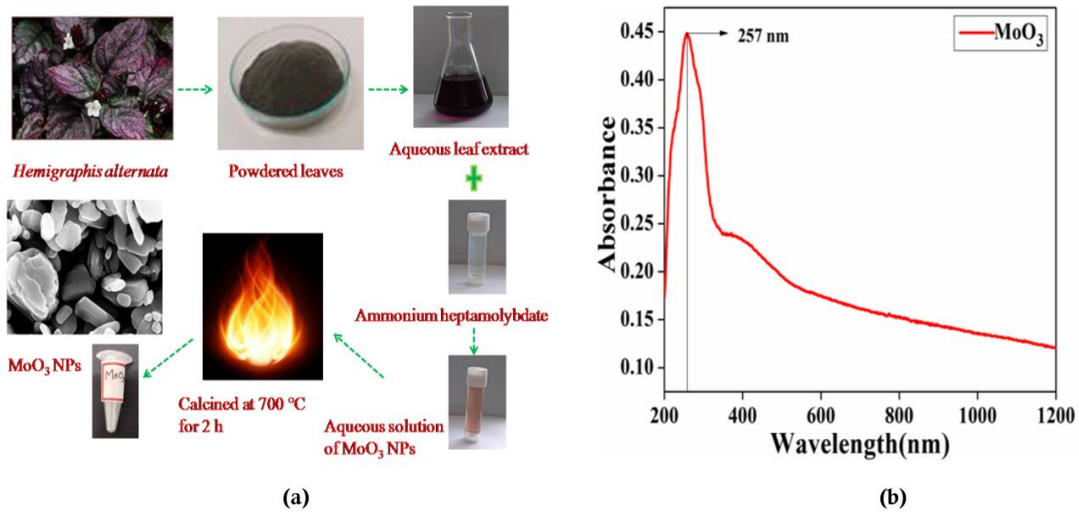

Figure 1. (a) Green synthesis of MoO3 NPs from HA leaf extract; **(b)** UV-Visible Spectroscopic analysis of green synthesized MoO3 NPs.

4.2. FTIR spectroscopy

The functional groups and bonds present in the green synthesized MoO_3 NPs were examined using FTIR spectroscopy, and the corresponding spectrum is shown in **Figure 2**. The band observed at 984 cm^{-1} indicates the presence of the orthorhombic MoO_3 phase, characterized by the terminal molybdenum to oxygen double bond [39]. The peaks at 635 cm^{-1}, 738 cm^{-1}, and 871 cm^{-1} correspond to the bending vibrational modes of Mo-O-Mo bonds and the stretching vibrations of Mo=O bonds [40,41]. The intense vibrations observed at 1952 cm^{-1} and 1077 cm^{-1}

are attributed to the stretching mode of oxygen with metal atoms. The presence of adsorbed water on the surface of MoO_3 is what causes these higher wavenumber bands. The remaining stretching modes are associated with the use of ammonium heptamolybdate as the precursor for the synthesis [42].

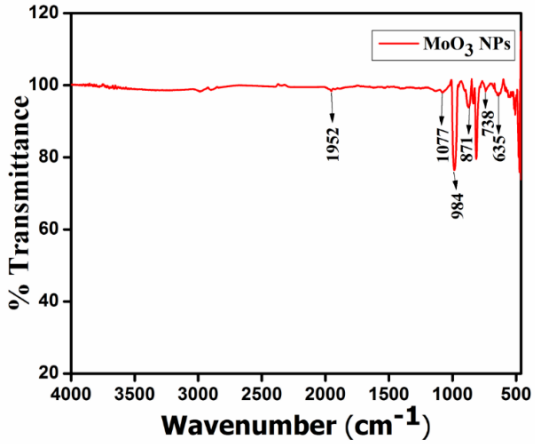

Figure 2. FTIR spectra of green synthesized MoO3 NPs using HA extract.

4.3. XRD

The XRD pattern of green synthesized MoO_3 NPs is presented in **Figure 3**. The prominent peaks observed at 12.7°, 23.1°, 25.6°, 27.1°, 29.7°, 33°, 33.7°, 35.5°, 38.5°, 39°, 45.6°, 46.4°, 49.2°, 50.9°, 52.7°, 56.2°, 58.8°, 64.3°, 69.4°, 72.8°, and 76.5° correspond to the crystallographic planes (020), (110), (040), (021), (130), (101), (041), (131), (160), (210), (002), (230), (080), (112), (081), (062), (202), (232), and (301). By utilizing JCPDS software, the XRD spectrum was compared to the reference card number 895108 from the Joint Committee on Powder Diffraction Standards (JCPDS), confirming the formation of MoO_3 NPs. The XRD analysis revealed that the green synthesized MoO_3 NPs exhibited an orthorhombic crystal structure and a high degree of crystallinity [39,42]. The Debye-Scherrer equation was used to calculate the average crystallite size of the green synthesized MoO_3 NPs.

$$D = k\lambda/(\beta\, cos\theta)$$

where D is the average crystallite size, k is the crystallite shape factor, λ is the wavelength of the X-ray source (1.5406 Å), β is the full width at half maximum (FWHM) in radians, and θ is the Bragg angle in radians. The average crystallite size (D) of the synthesized MoO_3 NPs was determined to be 61 nm.

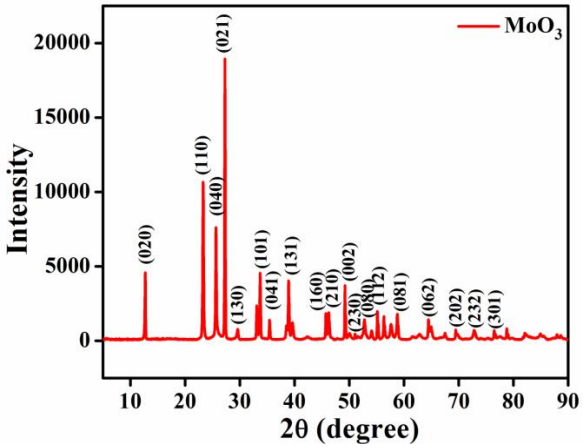

Figure 3. XRD pattern of the green synthesized MoO3 NPs using HA extract.

4.4. FESEM with EDAX analysis

The MoO_3 NPs exhibited an average grain size of approximately 478 nm and displayed irregular morphology, as depicted in **Figure 4a,b** [43]. The particle size was calculated using the ImageJ software and the particle size distribution histogram are given in **Figure 4c**. The NPs were observed to be agglomerated, forming clusters. The energy dispersive x-ray analysis (EDAX) spectrum provided information about the elemental composition of the synthesized product. It showed that the predominant elements present were molybdenum and oxygen. **Figure 4d** illustrates the atomic contents of molybdenum and oxygen based on the EDAX spectrum. No discernible impurity peaks were observed in the spectrum.

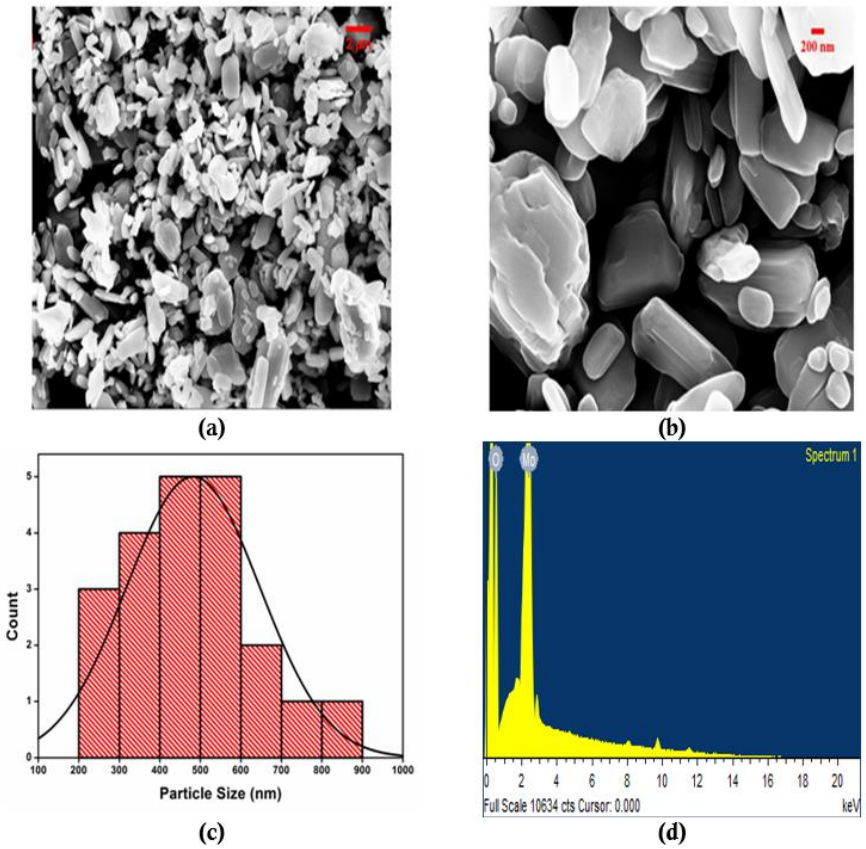

Figure 4. (a) High (2 µm) and **(b)** low (200 nm) magnification of FESEM images; **(c)** particle size distribution histogram; **(d)** EDAX spectrum of green synthesized MoO3 NPs using HA extract.

4.5. DLS and ZP

The optimization and synthesis of NPs are largely influenced by their particle size, which plays a significant role in their properties and applications. In this study, the stability and particle size distribution of MoO_3 NPs were assessed using ZP and DLS techniques. **Figure 5a,b** present the ZP and particle size distribution of the MoO_3 NPs, respectively. The ZP of the MoO_3 NPs was determined to be −17 mV. It is noteworthy that the green synthesis of MoO_3 NPs from *Lepidagathis cristata* leaf extract exhibited a zeta potential of −34.6 mV, indicating a higher level of stability [39]. The particle size distribution analysis revealed an estimated average particle size of 584 nm at a scattering angle of 90°. The polydispersity index value, a measure of the width of the size distribution, was found to be 26.14%. The larger particle size observed could be attributed to the presence of polyphenols or impurities within the NPs. The precise nature of these factors impacting particle size may require further research to clarify.

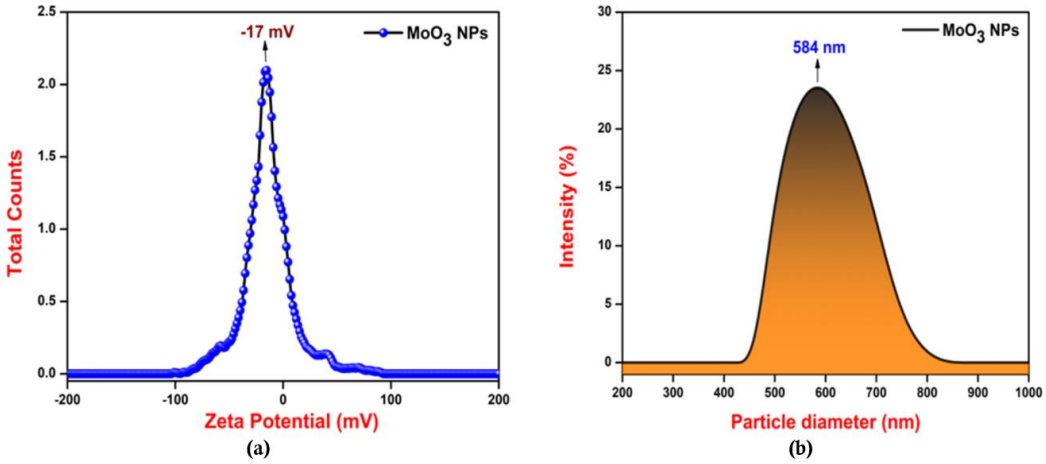

Figure 5. (a) Zeta potential; **(b)** particle size distribution of green synthesised MoO3 NPs using HA leaf extract.

4.6. TGA

The thermal stability of MoO_3 NPs was evaluated using thermogravimetric analysis. **Figure 6** presents the TGA and DTG curve, which plots the mass of the sample against the temperature. The thermogram of MoO_3 NPs exhibited a gradual weight loss, totaling approximately 13%, within the temperature range of 100 °C–600 °C. The initial weight loss at temperatures near 200 °C can be attributed to the evaporation of retained and adsorbed water.

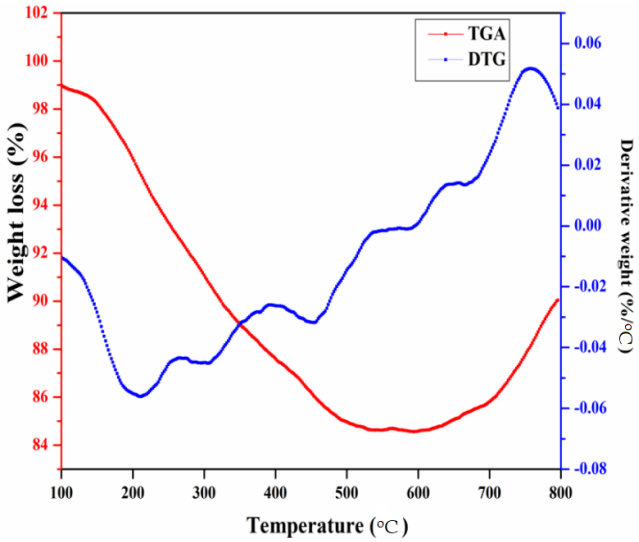

Figure 6. TGA and DTG curve of green synthesized MoO3 NPs using HA extract.

The maximum weight loss was obtained at this phase was confirmed by the major peaks of DTG curve. As the temperature increased, the organic compounds present in the NPs started to decompose, resulting in further weight loss. It is important to note that while some organic compounds can withstand temperatures up to 200 °C, the organic skeleton within the MoO_3 NPs disintegrated at higher temperatures [44,45]. This phenomenon explains the observed weight loss in the thermogram. However, there is a slight increase in mass by heating above 600 °C was observed, which could be a result of oxidation at high temperatures [46]. Overall, the TGA analysis provides insights into the thermal stability of the MoO_3 NPs and indicates their behavior under increasing temperatures, shedding light on their potential applications in various temperature-dependent processes.

4.7. Antioxidant activity

Aromatic and medicinal plants have long been utilized for their bioactive properties in therapeutic applications [27]. The estimation of radical scavenging activity of MoO_3 NPs was carried out using the DPPH and ABTS assays. A concentration of 2 mg/mL of synthesized MoO_3 NPs was employed, with ascorbic acid serving as the positive control. The DPPH assay is based on the reduction of the persistent free radical DPPH by antioxidants, forming the corresponding hydrazine. This technique provides a measure of the antioxidant potential [47]. Conversely, the ABTS assay involves the interaction between antioxidants and the oxidized ABTS radical cation, resulting in a decrease in the ABTS radical. This spectrophotometric technique is used to assess the radical scavenging activity [48]. **Figure 7a,b** present the radical scavenging activity of MoO_3 NPs as determined by the DPPH and ABTS assays, respectively. The MoO_3 NPs exhibited antioxidant activities of 60% ± 0.67%, 70.48% ± 0.12%, 82.25% ± 0.76%, and 89.53% ± 0.54% against DPPH, and 65.86% ± 0.61%, 71.15% ± 0.26%, 85.60% ± 0.46%, and 91.15% ± 0.54% against ABTS at various concentrations (0.5, 1, 1.5, and 2 mg/mL). These results indicate that the green synthesized MoO_3 NPs possess significant dose-dependent scavenging activity against free radicals. The percentage inhibition gradually increased in a dose-

dependent manner, reaching its maximum level. Fakhri and Nejad also reported the maximum inhibition of 82% at 1 mM and minimum inhibition of 55% at a 0.125 mM concentration stating the concentration-dependent antioxidant activity of MoO_3 NPs against ABTS radicals [48,49]. These findings highlight the potent antioxidant properties of the MoO_3 NPs, suggesting their potential application in combating oxidative stress-related disorders and promoting overall health.

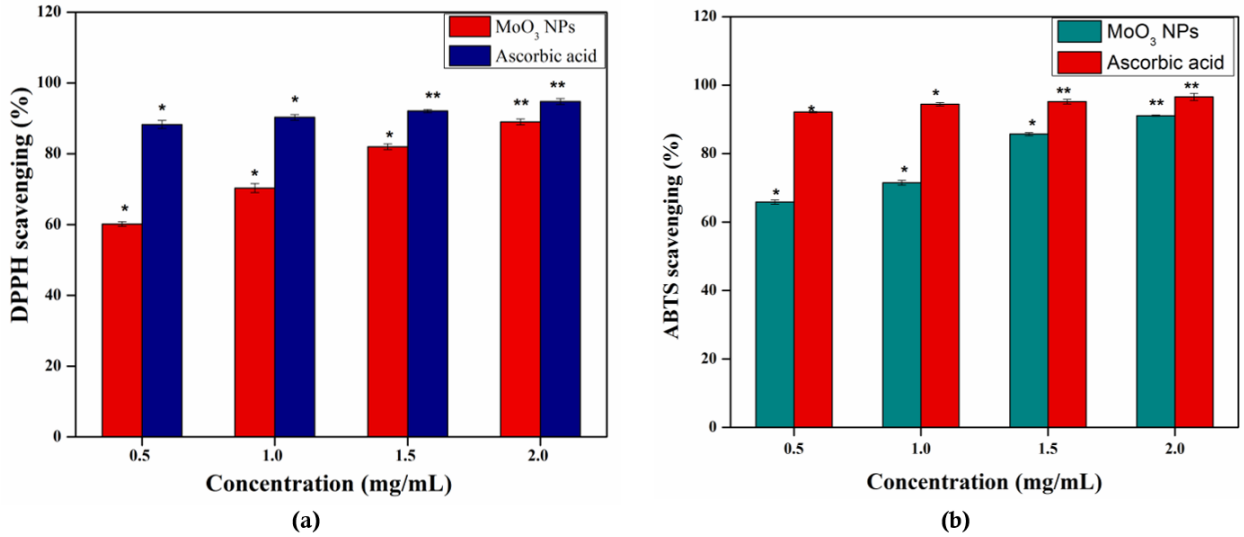

Figure 7. Free radical scavenging effects of green synthesized MoO3 NPs at various concentrations by **(a)** DPPH; **(b)** ABTS assays. Values are denoted as the mean ± SD; * denotes statistical difference at $p < 0.05$, and ** denotes $p < 0.01$.

4.8. Antimicrobial activity

4.8.1. Minimum inhibitory concentration (MIC)

The MIC is a crucial factor for assessing the susceptibility of a pathogen to antimicrobial agents. A lower MIC value indicates higher microbial susceptibility and more potent antimicrobial activity [50]. In the case of MoO_3 NPs, the minimum concentration required against *S. aureus* was determined to be 6.25 µg/mL, and MIC of the NPs against *P. aeruginosa*, was found to be 12.5 µg/mL. Another study on MoO_3 nanoplates revealed MIC values of 8 µg/mL against *E. coli* and 16 µg/mL against *Enterococcus faecalis* using microdilution method [51]. It is noteworthy that molybdenum, the primary component of MoO_3 NPs, has been identified as a non-toxic element, which makes MoO_3 NPs a promising candidate for biocidal coatings aimed at reducing bacterial contamination [52]. Determining the MIC value of any antibacterial agent is crucial for assessing its potential in therapeutic applications [53]. The observed low MIC values of MoO_3 NPs against *S. aureus* and *P. aeruginosa* highlight their potent antimicrobial activity and suggest their potential use as an effective antimicrobial agent. Further investigations are necessary to find out the mechanism of action and to explore the application of MoO_3 NPs in various antimicrobial strategies.

4.8.2. Antibacterial activity

The antibacterial activity of MoO_3 NPs was evaluated using the agar-well diffusion method against the bacteria *S. aureus* and *P. aeruginosa*, as illustrated in

Figure 8a. The zone of inhibition against *S. aureus* was determined to be 10 ± 0.75 mm, 14 ± 0.93 mm, and 18 ± 0.24 mm at concentrations of 0.25, 0.5, and 1 µg/mL, respectively. Similarly, for the gram-negative bacterium *P. aeruginosa*, the zone of inhibition was measured as 9 ± 0.26 mm, 13 ± 0.65 mm, and 16 ± 1.21 mm at the corresponding concentrations. In contrast, the positive control, Cefmetazole (30 µg), and MoO_3 NPs at a concentration of 0.125 µg/mL did not exhibit any zone of inhibition against these multi-drug resistant bacteria, as indicated in **Table 1**. These results suggest that the antibacterial activity of MoO_3 NPs is concentration-dependent. Fakhri and Nejad also reported concentration dependent bactericidal activity of MoO_3 against both gram-positive and gram-negative pathogens [49]. The observed antibacterial effects of MoO_3 NPs indicate their potential as an alternative therapeutic agent for combating bacterial infections caused by *S. aureus and P. aeruginosa*.

Table 1. Zone of inhibition(mm) of MoO3 NPs against bacterial pathogens (1) S. aureus and (2) P. aeruginosa.

Bacterial pathogen	Zone of inhibition (mm)				
	0.125 mg/mL	**0.25 mg/mL**	**0.5 mg/mL**	**1 mg/mL**	**Cefmetazole (30 µg)**
S. aureus	-	10 ± 0.98	14 ± 0.94	18 ± 0.78	-
P. aeruginosa	-	9 ± 0.32	13 ± 0.45	16 ± 0.62	-

4.8.3. Antifungal activity

The synthesized MoO_3 NPs were treated with different doses ranging from 0.125 to 1 mg/mL for their antifungal efficacy against strains of *A. niger* and *C. albicans*. The results, presented in **Table 2**, demonstrate a concentration dependent antifungal effect of MoO_3 NPs on both fungal strains. At a concentration of 1 mg/mL, MoO_3 NPs exhibited substantial inhibition zones of 23 mm and 29 mm against *A. niger* and *C. albicans*, respectively. However, at a lower concentration of 0.125 mg/mL, MoO_3 NPs only showed a modest inhibition zone of 12 mm against *C. albicans*, while no inhibition was observed against *A. niger*, as depicted in **Figure 8b**. The potent antifungal activity of MoO_3 NPs can be ascribed to their ability to disrupt hyphal growth, inhibit spore formation, and impede conidiospore germination through direct interactions with the fungi [54]. In a study by Kumari and Mangala, the antifungal activity of bulk and NPs of molybdenum trioxide against Aspergillus sp. was investigated. It was found that the bulk sample did not exhibit any activity at 100 µL, while MoO_3 NPs displayed zones of inhibition of 2 mm and 5 mm at concentrations of 200 µL and 300 µL, respectively, against Aspergillus sp [55]. Additionally, Vanathi et al. reported the antifungal activity of Eichhornia-mediated copper oxide NPs against *A. niger*, observing an inhibition zone of 18.33 mm at a concentration of 100 µg/mL [56]. Moreover, AgNPs synthesized from the aqueous extract of *L. acapulcensis* demonstrated inhibitory effects on *C. albicans*, with an inhibition zone of 19 ± 0.5 mm observed at a concentration of 0.25 µg/mL [57]. The observed antifungal activity of MoO_3 NPs against *A. niger* and *C. albicans* highlights their potential as effective agents for combating fungal infections.

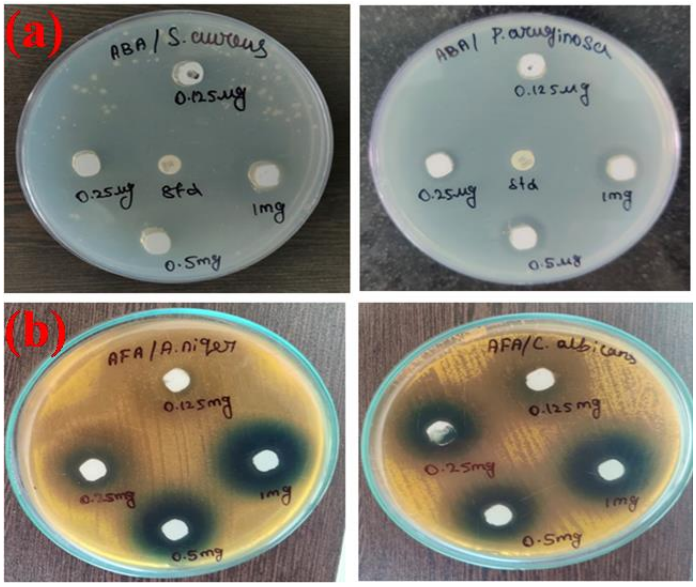

Figure 8. (a) Antibacterial activity of green synthesized MoO3 NPs against (1) S. aureus and (2) P. aeruginosa, Cefmetazole was used as standard; **(b)** antifungal activity of green synthesized MoO3 NPs against (3) Aspergillus niger and (4) Candida albicans.

Table 2. Zone of inhibition (mm) of green synthesized MoO3 NPs against fungal pathogens (1) Aspergillus niger and (2) Candida albicans.

Fungal pathogen	Zone of inhibition (mm)			
	0.125 mg/mL	**0.25 mg/mL**	**0.5 mg/mL**	**1 mg/mL**
Aspergillus niger	-	11 ± 0.12	18 ± 0.34	23 ± 1.76
Candida albicans	12 ± 0.97	19 ± 1.42	25 ± 1.66	29 ± 1.98

4.8.4. Time dynamic assay

To determine the rate of bacterial cell reduction after treatment with green synthesized MoO_3 NPs at various time intervals, the time-dependent antibacterial activity of MoO_3 NPs against *S. aureus* and *P. aeruginosa* was examined. The increased bacterial reduction rate with the duration of exposure to MoO_3 NPs, indicating a positive correlation between the duration of treatment and the bactericidal effect are depicted in **Figure 9**. Significant bacterial reduction was observed at various time intervals. At the MIC of both *S. aureus* and *P. aeruginosa*, a reduction of over 50% in bacterial count was observed after 4 h of exposure. Specifically, *S. aureus* exhibited a reduction rate of 56.9%, while *P. aeruginosa* showed a reduction rate of 52.89% after 4 h. This discrepancy in susceptibility to MoO_3 NPs between gram-positive and gram-negative bacteria can be attributed to the difference in structural compositions of the bacterial cell walls. Gram-negative bacteria possess an additional outer membrane that contains lipopolysaccharides (LPS), which enhances the barrier functions of the outer membrane and contributes to increased bacterial resistance compared to gram-positive bacteria [58,59]. In a study by da Silva et al. the antibacterial activity of ZnO NPs against *S. aureus* and *E. coli* was investigated. It was observed that gram-negative bacteria, exhibited lower sensitivity to ZnO NPs compared to gram-positive bacteria, highlighting the greater

resistance of gram-negative bacteria to nanoparticle based antibacterial agents [60]. The findings suggest that MoO_3 NPs possess time-dependent antibacterial activity, with a more pronounced effect observed over extended exposure periods. The differential response of gram-positive and gram-negative bacteria to MoO_3 NPs underscores the importance of understanding the unique characteristics of bacterial cell walls when designing effective antibacterial strategies.

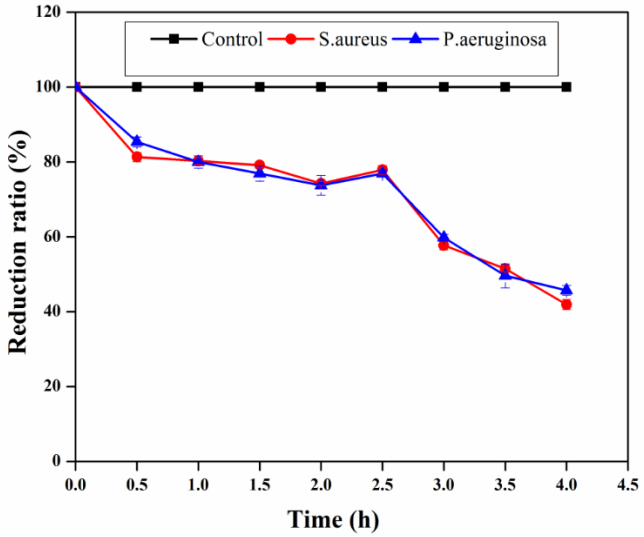

Figure 9. Time-dynamic antibacterial property of green synthesized MoO3 NPs at MIC of S. aureus and P. aeruginosa for 4 h.

4.8.5. Assessment of protein leakage and reducing sugar

The antibacterial activity of MoO_3 NPs was assessed by measuring the leakage of biomolecules, specifically proteins and reducing sugars, which serve as representative indicators of cell content leakage. The effect of MoO_3 NPs on biomolecule leakage was evaluated over a 4 h period, during which the treated bacterial cells experienced cell death and disruption of the cell envelope. The control samples, which were left untreated, exhibited minimal increase in the leakage of biomolecules, as depicted in **Figure 10a**. In the case of *S. aureus*, the protein leakage from the cell membranes was measured at 154.88 µg/mL, while the untreated control exhibited a protein leakage of 20.03 µg/mL. For *P. aeruginosa*, the treated group displayed a protein leakage of 130 µg/mL compared to 14.9 µg/mL in the untreated group. Similarly, significant leakage of reducing sugars was observed in both *S. aureus* and *P. aeruginosa* after 4 h of treatment. **Figure 10b** illustrates the results, with a notable reducing sugar leakage of 61.69 µg/mL and 53.9 µg/mL in the treated groups of *S. aureus* and *P. aeruginosa*, respectively. The observed increase in protein and reducing sugar leakage in the MoO_3 NPs treated cells compared to the control indicates that MoO_3 NPs enhance the permeability of bacterial cell membranes. The disintegration of the cell walls consequently leads to the leakage of endogenous proteins and reducing sugars, resulting in bacterial cell death. Thus, it is evident from the leakage of biomolecules that MoO_3 NPs possess strong antibacterial activity.

Furthermore, compared to chemically synthesized nanoparticles, green nanoparticles demonstrate a higher affinity and stronger adhesion to bacterial cell membranes, thereby supporting their superior antibacterial effect [61]. Consequently, the leakage of proteins and sugars from the *S. aureus* cells were comparatively higher than *P. aeruginosa* when treated with MoO_3 NPs. A case study involving *S. aureus* and *E. coli* as models for gram-positive and gram-negative bacteria, respectively, revealed that after 6 h of exposure to AgNPs, more proteins leaked through the *S. aureus* membranes than the *E. coli* membranes, indicating that gram-positive bacteria are generally more sensitive to antibacterial agents than gram-negative bacteria [62]. These findings highlight the ability of MoO_3 NPs to disrupt bacterial cell membranes, leading to biomolecule leakage and ultimately causing bacterial death.

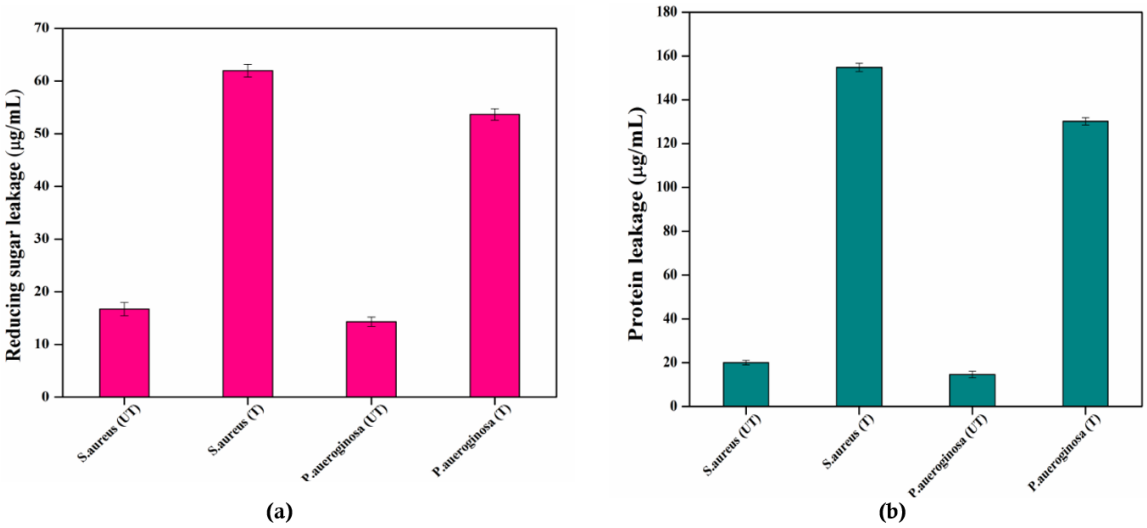

Figure 10. Effects of MoO3 NPs on leakage of biomolecules. **(a)** Leakage of proteins and **(b)** leakage of reducing sugars from S. aureus and P. aeruginosa for 4 h. Each value is expressed as mean ± S.D., $n = 3$ independent experiments.

4.9. Hemolysis assay

Hemolysis assay was used to assess the therapeutic effectiveness of MoO_3 NPs on human erythrocytes. When nanoparticles are introduced into the blood stream, they interact with blood components, which can have potential implications. Erythrocytes impart vital role in hemostasis and thrombosis owing to their rheological properties and abundance in the blood [63]. NPs can induce oxidative stress and physiochemical interactions with erythrocytes, leading to hemolysis and cell denaturation [64]. Hemolysis occurs when the cell membrane ruptures, resulting in the leakage of hemoglobin (Hb) into the surrounding solution [65]. Therefore, assessing the hemocompatibility of green synthesized MoO_3 NPs is essential before considering their application in therapeutic contexts.

The hemolytic activity of green synthesized MoO_3 NPs was examined at concentrations ranging from 25, 50, 75, 100 µg/mL are depicted in **Figure 11**. The hemolytic activity showed a concentration-dependent trend, likely due to increased oxidative stress on erythrocytes. The erythrocytes incubated with various concentrations (25–100 µg/mL) displayed hemolysis percentages of 2.22%, 3.65%,

3.86%, and 4.13% respectively. These values indicate that the damage caused by the MoO_3 NPs was within the non-hemolytic range (< 5%), as compared to the 100% hemolysis displayed by cells treated with 0.1% Triton X-100 (positive control). Standardization efforts in the field of nanotechnology, such as those by the American Society for Testing and Materials (ASTM) International, recognize the interaction between NPs and the immune system as a standard requirement [66]. Hemolysis rates below 5% are considered safe according to the ASTM [67]. In contrast, ZnO NPs demonstrated hemolysis rates of 7.7% and 75.3% at concentrations of 300 and 600 µg/mL, respectively [68]. Therefore, the synthesized MoO_3 NPs exhibited non-hemolytic and non-toxic effects on human erythrocytes.

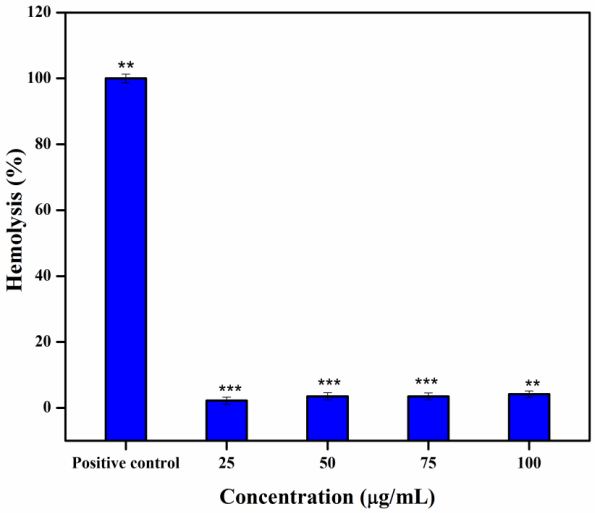

Figure 11. Hemocompatability of green synthesized MoO3 NPs at various concentrations (25–100 µg/mL) was evaluated by in vitro hemolysis assay in human erythrocytes. Each experiment was performed in triplicates, and data are presented as mean ± SD.** denotes $P < 0.01$, and *** denotes $P < 0.001$.

4.10. Cytotoxicity analysis

4.10.1. MTT assay

The cytotoxicity of MoO_3 NPs was assessed using the MTT assay with mouse fibroblast L929 cells. Cell viability was measured after exposing the cells to concentrations of 25, 50, 75, and 100 µg/µL of MoO_3 NPs for 24 h. The results, shown in **Figure 12**, indicated that cell viability decreased with higher concentrations of MoO_3 NPs. At concentrations below 50 µg/mL, the exposed cells exhibited more than 95% cell viability, while at higher concentrations, the viability decreased. Specifically, cell viabilities were recorded as 99%, 96%, 94.5%, and 93% for concentrations of 25, 50, 75, and 100 µg/µL respectively. Siddiqui et al. reported that low doses of MoO_3 NPs did not significantly reduce cell viability [69]. Furthermore, the biocompatibility of MoO_3 NPs falls within the acceptable limits defined by ISO-10993−5 [70]. These findings suggest that the cytotoxic effects of MoO_3 NPs are concentration dependent, with lower concentrations demonstrating higher cell viability. Therefore, MoO_3 NPs synthesized using green methods hold promise for potential biocompatible applications.

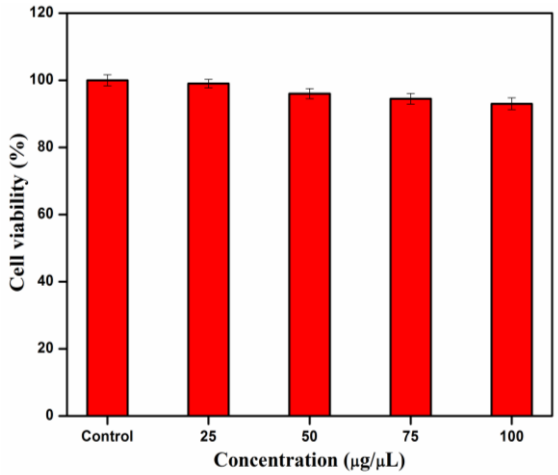

Figure 12. Graph showing percentage of cell viability at different concentrations of MoO3 NPs in L929 mouse fibroblast cell line by MTT assay. The cytotoxic effect was compared to control. Each value is expressed as mean ± S.D., *n* = 3 independent experiments.

4.10.2. Scratch assay

The effect of MoO_3 NPs on cell migration during wound closure was examined using an in vitro scratch assay. The wound healing efficacy was evaluated at 12 h and 24 h, as depicted in **Figure 13**. In comparison to the control group, the scratch region treated with MoO_3 NPs showed remarkable wound closure. In the control group, only 20% of fibroblast cellular migration towards scratched area at 12 h and 55% of migration at 24 h was observed. In contrast, the nanoparticle treated group established a concentration-dependent increase in the rate of cell migration. In 24 h, 89% of the wound had closed at a concentration of 25 µg/µL of MoO_3 NPs. For the cells treated with 50 µg/µL, wound closure reached 90% at 12 h and 96% at 24 h are shown in **Figure 14**. The enhancement in cell mass following the scratch can be attributed to the active proliferation and migration of fibroblast cells towards the wound area. Indrakumar et al. [15] investigated the therapeutic efficacy of MoO_3 NPs incorporated into collagen scaffolds in wistar rats. The fabricated MoO_3-collagen scaffolds containing 50µg/mL of MoO_3 NPs exhibited a significant migration rate compared to the collagen scaffolds alone. The wistar rats treated with MoO_3 NPs loaded collagen scaffolds demonstrated complete healing of the wounded tissue in approximately 15 days, highlighting the tissue-restorative properties of MoO_3 NPs. Additionally, it has been reported that low concentrations of molybdenum possess angiogenic abilities [71]. Overall, these findings signify that MoO_3 NPs have the efficacy to promote wound healing by facilitating cell migration and tissue regeneration.

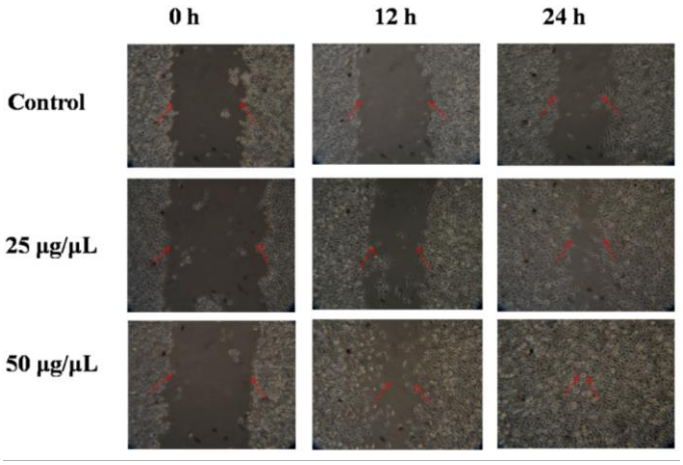

Figure 13. Healing of scratch wounds using two different concentrations (25 and 50 µg/µL) of MoO3 NPs at 12 h and 24 h.

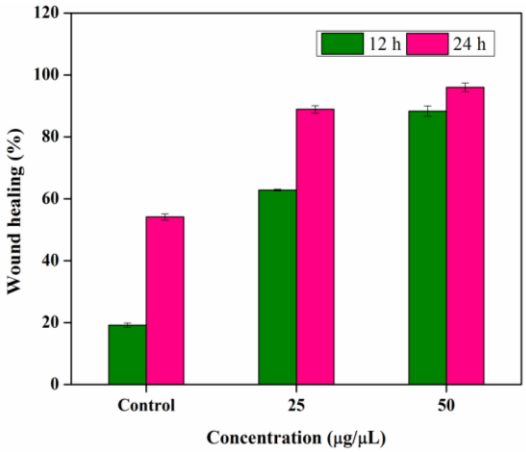

Figure 14. Graph represents the percentage of wound closure using two different concentrations (25 and 50 µg/µL) of MoO3 NPs at 12 h and 24 h. The experiments were performed in triplicates, and data are presented as mean ± SD.

5. Conclusion

The results of the present investigation demonstrated the remarkable antioxidant and antimicrobial activities of green synthesized MoO_3 NPs using HA leaves extract, specifically targeting skin infection-causing pathogens. Importantly, the cytotoxicity evaluation on L929 mouse fibroblast cells revealed the biocompatibility of MoO_3 NPs, as no significant reduction in cell viability was observed even at a concentration of 100 µg/µL. Moreover, the in vitro scratch assay provided evidence that MoO_3 NPs facilitated cell migration and exhibited significant wound healing efficacy, indicating their potential application in tissue regeneration and wound healing processes. These findings collectively emphasize the suitability of plant extract-mediated synthesis of MoO_3 NPs for incorporation into biopolymers or the formulation of new biomaterials. The green synthesis approach not only ensures eco-friendliness but also yields biocompatible and antimicrobial nanomaterials, making them attractive for various biomedical applications. However, to fully assess their long-term effectiveness, safety, and interactions with the human body, further comprehensive studies are warranted.

Author contributions: Conceptualization, AS and SS; methodology, AS and SS; software, AS and SS; validation, AS and SS; formal analysis, AS and SS; investigation, AS and SS; resources, AS and SS; data curation, AS and SS; writing—original draft preparation, AS and SS; writing—review and editing, AS and SS; visualization, AS and SS; supervision, SS; project administration, SS; funding acquisition, SS. All authors have read and agreed to the published version of the manuscript.

Funding: This research was funded by DBT, India for the financial support provided by the Ramalingaswami Re-entry fellowship, grant number No.BT/RLF/Re-entry/55/2013.

Acknowledgments: The author Subramaniam Sadhasivam acknowledges DBT, India for the financial support provided by the Ramalingaswami Re-entry fellowship (Order No.BT/RLF/Re-entry/55/2013).

Conflict of interest: The authors declare no conflict of interest.

References

1. Ahn EY, Jin H, Park Y. Assessing the antioxidant, cytotoxic, apoptotic and wound healing properties of silver nanoparticles green-synthesized by plant extracts. Materials Science and Engineering: C 2019; 101: 204–216. doi: 10.1016/j.msec.2019.03.095
2. Ahmed HE, Iqbal Y, Aziz MH, et al. Green synthesis of CeO_2 nanoparticles from the Abelmoschus esculentus extract: Evaluation of antioxidant, anticancer, antibacterial, and wound-healing activities. Molecules 2021; 26(15): 4659. doi: 10.3390/molecules26154659
3. Chenthamara D, Subramaniam S, Ramakrishnan SG, et al. Therapeutic efficacy of nanoparticles and routes of administration. Biomaterials Research 2019; 23(1): 20. doi: 10.1186/s40824-019-0166-x
4. Selvi RT, Prasanna APS, Niranjan R, et al. Metal oxide curcumin incorporated polymer patches for wound healing. Applied Surface Science 2018; 449: 603–609. doi: 10.1016/j.apsusc.2018.01.143
5. Séby F. Chapter eleven—Metal and metal oxide nanoparticles in cosmetics and skin care products. Comprehensive Analytical Chemistry 2021; 93: 381–427. doi: 10.1016/bs.coac.2021.02.009
6. Soltys L, Olkhovyy O, Tatarchuk T, Naushad M. Green synthesis of metal and metal oxide nanoparticles: Principles of green chemistry and raw materials. Magnetochemistry 2021; 7(11): 145. doi: 10.3390/magnetochemistry7110145
7. Jeevanandam J, Kiew SF, Boakye-Ansah S, et al. Green approaches for the synthesis of metal and metal oxide nanoparticles using microbial and plant extracts. Nanoscale 2022; 14(7): 2534–2571. doi: 10.1039/d1nr08144f
8. Ishak NAIM, Kamarudin SK, Timmiati SN. Green synthesis of metal and metal oxide nanoparticles via plant extracts: An overview. Materials Research Express 2019; 6(11): 112004. doi: 10.1088/2053-1591/ab4458
9. Mobaraki F, Momeni M, Yazdi MET, et al. Plant-derived synthesis and characterization of gold nanoparticles: Investigation of its antioxidant and anticancer activity against human testicular embryonic carcinoma stem cells. Process Biochemistry 2021; 111: 167–177. doi: 10.1016/j.procbio.2021.09.010
10. Namvar F, Rahman H, Mohamad R, et al. Cytotoxic effect of magnetic iron oxide nanoparticles synthesized via seaweed aqueous extract. International Journal of Nanomedicine 2014; 9(1): 2479. doi: 10.2147/IJN.S59661
11. Vinodhini S, Vithiya BSM, Prasad TAA. Green synthesis of palladium nanoparticles using aqueous plant extracts and its biomedical applications. Journal of King Saud University-Science 2022; 34(4): 102017. doi: 10.1016/j.jksus.2022.102017
12. Marimuthu M, Kumar BP, Salomi LM, et al. Methylene blue-fortified molybdenum trioxide nanoparticles: Harnessing radical scavenging property. ACS Applied Materials & Interfaces 2018; 10(50): 43429–43438. doi: 10.1021/acsami.8b15841
13. Yoshida M, Hattori H, Ôta S, et al. Molybdenum balance in healthy young Japanese women. Journal of Trace Elements in Medicine and Biology 2006; 20(4): 245–252. doi: 10.1016/j.jtemb.2006.07.004

14. Indrakumar J, Korrapati PS. Steering efficacy of nano molybdenum towards cancer: Mechanism of action. Biological Trace Element Research 2020; 194: 121–134. doi: 10.1007/s12011-019-01742-2
15. Indrakumar J, Balan P, Murali P, et al. Applications of molybdenum oxide nanoparticles impregnated collagen scaffolds in wound therapeutics. Journal of Trace Elements in Medicine and Biology 2022; 72: 126983. doi: 10.1016/j.jtemb.2022.126983
16. Lopes E, Piçarra S, Almeida PL, et al. Bactericidal efficacy of molybdenum oxide nanoparticles against antimicrobial-resistant pathogens. Journal of Medical Microbiology 2018; 67(8): 1042–1046. doi: 10.1099/jmm.0.000789
17. Hussain SM, Hess KL, Gearhart JM, et al. In vitro toxicity of nanoparticles in BRL 3A rat liver cells. Toxicology in Vitro 2005; 19(7): 975–983. doi: 10.1016/j.tiv.2005.06.034
18. Fazio E, Speciale A, Spadaro S, et al. Evaluation of biological response induced by molybdenum oxide nanocolloids on in vitro cultured NIH/3T3 fibroblast cells by micro-Raman spectroscopy. Colloids and Surfaces B: Biointerfaces 2018; 170: 233–241. doi: 10.1016/j.colsurfb.2018.06.028
19. Sasidharan S, Pottail L. Anti-bacterial and skin-cancer activity of AuNP, rGO and AuNP-rGO composite using Hemigraphis alternata (Burm.F.) T. Anderson. Biocatalysis and Agricultural Biotechnology 2020; 25: 101596. doi: 10.1016/j.bcab.2020.101596
20. Koshy J, Sangeetha D. Hemigraphis alternata leaf extract incorporated agar/pectin-based bio-engineered wound dressing materials for effective skin cancer wound care therapy. Polymers 2022; 15(1): 115. doi: 10.3390/polym15010115
21. Sreekumar D, Bhasker S, Devi PR, Mohankumar C. Wound healing potency of Hemigraphis alternata (Burm.f) T. Anderson leaf extract (HALE) with molecular evidence. Indian Journal of Experimental Biology 2021; 58: 236–245.
22. Zumsteg IS, Weckerle CS. Bakera, a herbal steam bath for postnatal care in Minahasa (Indonesia): Documentation of the plants used and assessment of the method. Journal of Ethnopharmacology 2007; 111(3): 641–650. doi: 10.1016/j.jep.2007.01.016
23. Annapoorna M, Kumar PT, Lakshman LR, et al. Biochemical properties of Hemigraphis alternata incorporated chitosan hydrogel scaffold. Carbohydrate Polymers 2013; 92(2): 1561–1565. doi: 10.1016/j.carbpol.2012.10.041
24. Rahman SMM, Atikullah M, Islam MN, et al. Anti-inflammatory, antinociceptive and antidiarrhoeal activities of methanol and ethyl acetate extract of Hemigraphis alternata leaves in mice. Clinical Phytoscience 2019; 5: 16. doi: 10.1186/s40816-019-0110-6
25. Abazari M, Akbari T, Hasani M, et al. Polysaccharide-based hydrogels containing herbal extracts for wound healing applications. Carbohydrate Polymers 2022; 294: 119808. doi: 10.1016/j.carbpol.2022.119808
26. Kanneganti A, Manasa C, Doddapaneni P. A sustainable approach towards synthesis of MoO_3 nanoparticles using citrus limetta pith extract. International Journal of Engineering and Advanced Technology 2014; 3(5): 128–130.
27. Prasathkumar M, Anisha S, Dhrisya C, et al. Therapeutic and pharmacological efficacy of selective Indian medicinal plants—A review. Phytomedicine Plus 2021; 1(2): 100029. doi: 10.1016/j.phyplu.2021.100029
28. Rajkumar T, Sapi A, Das G, et al. Biosynthesis of silver nanoparticle using extract of Zea mays (corn flour) and investigation of its cytotoxicity effect and radical scavenging potential. Journal of Photochemistry and Photobiology B: Biology 2019; 193: 1–7. doi: 10.1016/j.jphotobiol.2019.01.008
29. Mogana R, Adhikari A, Tzar MN, et al. Antibacterial activities of the extracts, fractions and isolated compounds from Canarium patentinervium Miq. against bacterial clinical isolates. BMC Complementary Medicine and Therapies 2020; 20: 55. doi: 10.1186/s12906-020-2837-5
30. Gokulakrishnan R, Ravikumar S, Raj JA. In vitro antibacterial potential of metal oxide nanoparticles against antibiotic resistant bacterial pathogens. Asian Pacific Journal of Tropical Disease 2012; 2(5): 411–413. doi: 10.1016/S2222-1808(12)60089-9
31. Devi HS, Boda MA, Shah MA, Shah MA. Green synthesis of iron oxide nanoparticles using Platanus orientalis leaf extract for antifungal activity. Green Processing and Synthesis 2019; 8(1): 38–45. doi: 10.1515/gps-2017-0145
32. Zhao R, Lv M, Li Y, et al. Stable nanocomposite based on PEGylated and silver nanoparticles loaded graphene oxide for long-term antibacterial activity. ACS Applied Materials & Interfaces 2017; 9(18): 15328–15341. doi: 10.1021/acsami.7b03987
33. Li WR, Xie XB, Shi QS, et al. Antibacterial activity and mechanism of silver nanoparticles on Escherichia coli. Applied Microbiology and Biotechnology 2010; 85: 1115–1122. doi: 10.1007/s00253-009-2159-5

34. Sulaiman CT, Gopalakrishnan VK. Radical scavenging and in-vitro hemolytic activity of aqueous extracts of selected acacia species. Journal of Applied Pharmaceutical Science 2013; 3(3): 109–111. doi: 10.7324/JAPS.2013.30321
35. Prasathkumar M, Raja K, Vasanth K, et al. Phytochemical screening and in vitro antibacterial, antioxidant, anti-inflammatory, anti-diabetic, and wound healing attributes of Senna auriculata (L.) Roxb. leaves. Arabian Journal of Chemistry 2021; 14(9): 103345. doi: 10.1016/j.arabjc.2021.103345
36. Prasathkumar M, Anisha S, Khusro A, et al. Anti-pathogenic, anti-diabetic, anti-inflammatory, antioxidant, and wound healing efficacy of Datura metel L. leaves. Arabian Journal of Chemistry 2022; 15(9): 104112. doi: 10.1016/j.arabjc.2022.104112
37. Hajiashrafi S, Motakef-Kazemi N. Green synthesis of zinc oxide nanoparticles using parsley extract. Nanomedicine Research Journal 2018; 3(1): 44–50. doi: 10.22034/nmrj.2018.01.007
38. Ganguly A, George R. Synthesis, characterization and gas sensitivity of MoO_3 nanoparticles. Bulletin of Materials Science 2007; 30(2): 183–185. doi: 10.1007/s12034-007-0033-6
39. Nunna GP, Siddarapu HK, Nimmagadda VV, et al. Biogenic synthesis of high-performance α-MoO_3 nanoparticles from tryptophan derivatives for antimicrobial agents and electrode materials of supercapacitors. International Journal of Energy Research 2023; 2023: 6715319. doi: 10.1155/2023/6715319
40. Gowtham B, Ponnuswamy V, Pradeesh G, et al. MoO_3 overview: Hexagonal plate-like MoO_3 nanoparticles prepared by precipitation method. Journal of Materials Science: Materials in Electronics 2018; 29(8): 6835–6843. doi: 10.1007/s10854-018-8670-7
41. Myachina M, Gavrilova N, Nazarov V. Formation of molybdenum blue nanoparticles in the organic reducing area. Molecules 2021; 26(15): 4438. doi: 10.3390/molecules26154438
42. Mamatha KM, Murthy VS, Ravikumar CR, et al. Facile green synthesis of Molybdenum oxide nanoparticles using Centella Asiatica plant: Its photocatalytic and electrochemical lead sensor applications. Sensors International 2022; 3: 100153. doi: 10.1016/j.sintl.2021.100153
43. Prakash NG, Dhananjaya M, Lakshmi NA, Hussain OM. Green synthesis of molybdenum trioxide nanoparticles using Lepidagathiscristata leaf extract for supercapacitor applications. In: Proceedings of the International Meeting on Energy Storage Devices and Industry-Academia Conclave; 10–12 December 2018; Roorkee, India. p. 110.
44. Kothaplamoottil Sivan S, Padinjareveetil AKK, Padil VVT, et al. Greener assembling of MoO_3 nanoparticles supported on gum arabic: Cytotoxic effects and catalytic efficacy towards reduction of p-nitrophenol. Clean Technologies and Environmental Policy 2019; 21(8): 1549–1561. doi: 10.1007/s10098-019-01726-9
45. Bhuiyan MSH, Miah MY, Paul SC, et al. Green synthesis of iron oxide nanoparticle using Carica papaya leaf extract: Application for photocatalytic degradation of remazol yellow RR dye and antibacterial activity. Heliyon 2020; 6(8): e04603. doi: 10.1016/j.heliyon.2020.e04603
46. Sackey J, Nwanya AC, Bashir AKH, et al. Electrochemical properties of Euphorbia pulcherrima mediated copper oxide nanoparticles. Materials Chemistry and Physics 2020; 244: 122714. doi: 10.1016/j.matchemphys.2020.122714
47. Martínez-Cabanas M, López-García M, Rodríguez-Barro P, et al. Antioxidant capacity assessment of plant extracts for green synthesis of nanoparticles. Nanomaterials 2021; 11(7): 1679. doi: 10.3390/nano11071679
48. Al-Radadi NS. Facile one-step green synthesis of gold nanoparticles (AuNp) using licorice root extract: Antimicrobial and anticancer study against HepG2 cell line. Arabian Journal of Chemistry 2021; 14(2): 102956. doi: 10.1016/j.arabjc.2020.102956
49. Fakhri A, Nejad PA. Antimicrobial, antioxidant and cytotoxic effect of Molybdenum trioxide nanoparticles and application of this for degradation of ketamine under different light illumination. Journal of Photochemistry and Photobiology B: Biology 2016; 159: 211–217. doi: 10.1016/j.jphotobiol.2016.04.002
50. Arsène MMJ, Podoprigora IV, Davares AKL, et al. Antibacterial activity of grapefruit peel extracts and green-synthesized silver nanoparticles. Veterinary World 2021; 14(5): 1330–1341. doi: 10.14202/vetworld.2021.1330-1341
51. Krishnamoorthy K, Veerapandian M, Yun K, Kim SJ. New function of molybdenum trioxide nanoplates: Toxicity towards pathogenic bacteria through membrane stress. Colloids and Surfaces B: Biointerfaces 2013; 112: 521–524. doi: 10.1016/j.colsurfb.2013.08.026
52. Tétault N, Gbaguidi-Haore H, Bertrand X, et al. Biocidal activity of metalloacid-coated surfaces against multidrug-resistant microorganisms. Antimicrobial Resistance and Infection Control 2012; 1: 35. doi: 10.1186/2047-2994-1-35

53. Krishnamoorthy K, Premanathan M, Veerapandian M, Kim SJ. Nanostructured molybdenum oxide-based antibacterial paint: Effective growth inhibition of various pathogenic bacteria. Nanotechnology 2014; 25(31): 315101. doi: 10.1088/0957-4484/25/31/315101
54. Chen J, Wu L, Lu M, et al. Comparative study on the fungicidal activity of metallic MgO nanoparticles and macroscale MgO against soilborne fungal phytopathogens. Frontiers in Microbiology 2020; 11: 365. doi: 10.3389/fmicb.2020.00365
55. Kumari J, Mangala P. Fabrication and characterization of molybdenum trioxide nanoparticles and their anticancer, antibacterial and antifungal activities. Malaysian Journal of Chemistry 2022; 24(1): 36–53.
56. Vanathi P, Rajiv P, Sivaraj R. Synthesis and characterization of Eichhornia-mediated copper oxide nanoparticles and assessing their antifungal activity against plant pathogens. Bulletin of Materials Science 2016; 39(5): 1165–1170. doi: 10.1007/s12034-016-1276-x
57. Garibo D, Borbón-Nuñez HA, de León JND, et al. Green synthesis of silver nanoparticles using Lysiloma acapulcensis exhibit high-antimicrobial activity. Scientific Reports 2020; 10: 12805. doi: 10.1038/s41598-020-69606-7
58. Gudkov SV, Burmistrov DE, Serov DA, et al. A mini review of antibacterial properties of ZnO nanoparticles. Frontiers in Physics 2021; 9: 641481. doi: 10.3389/fphy.2021.641481
59. Kashef N, Huang YY, Hamblin MR. Advances in antimicrobial photodynamic inactivation at the nanoscale. Nanophotonics 2017; 6(5): 853–879. doi: 10.1515/nanoph-2016-0189
60. da Silva BL, Caetano BL, Chiari-Andréo BG, et al. Increased antibacterial activity of ZnO nanoparticles: Influence of size and surface modification. Colloids and Surfaces B: Biointerfaces 2019; 177: 440–447. doi: 10.1016/j.colsurfb.2019.02.013
61. Qayyum S, Oves M, Khan AU. Obliteration of bacterial growth and biofilm through ROS generation by facilely synthesized green silver nanoparticles. PloS One 2017; 12(8): e0181363. doi: 10.1371/journal.pone.0181363
62. Gomaa EZ. Silver nanoparticles as an antimicrobial agent: A case study on Staphylococcus aureus and Escherichia coli as models for gram-positive and gram-negative bacteria. The Journal of General and Applied Microbiology 2017; 63(1): 36–43. doi: 10.2323/jgam.2016.07.004
63. de la Harpe KM, Kondiah PPD, Choonara YE, et al. The hemocompatibility of nanoparticles: A review of cell-nanoparticle interactions and hemostasis. Cells 2019; 8(10): 1209. doi: 10.3390/cells8101209
64. Ashokraja C, Sakar M, Balakumar S. A perspective on the hemolytic activity of chemical and green-synthesized silver and silver oxide nanoparticles. Materials Research Express 2017; 4(10): 105406. doi: 10.1088/2053-1591/aa90f2
65. Selvakumar P, Sithara R, Viveka K, Sivashanmugam P. Green synthesis of silver nanoparticles using leaf extract of Acalypha hispida and its application in blood compatibility. Journal of Photochemistry and Photobiology B: Biology 2018; 182: 52–61. doi: 10.1016/j.jphotobiol.2018.03.018
66. Dobrovolskaia MA, Aggarwal P, Hall JB, McNeil SE. Preclinical studies to understand nanoparticle interaction with the immune system and its potential effects on nanoparticle biodistribution. Molecular Pharmaceutics 2008; 5(4): 487–495. doi: 10.1021/mp800032f
67. Vanaraj S, Keerthana BB, Preethi K. Biosynthesis, characterization of silver nanoparticles using quercetin from Clitoria ternatea L to enhance toxicity against bacterial biofilm. Journal of Inorganic and Organometallic Polymers and Materials 2017; 27: 1412–1422. doi: 10.1007/s10904-017-0595-8
68. Mahanta S, Prathap S, Ban DK, Paul S. Protein functionalization of ZnO nanostructure exhibits selective and enhanced toxicity to breast cancer cells through oxidative stress-based cell death mechanism. Journal of Photochemistry and Photobiology B: Biology 2017; 173: 376–388. doi: 10.1016/j.jphotobiol.2017.06.015
69. Siddiqui MA, Saquib Q, Ahamed M, et al. Molybdenum nanoparticles-induced cytotoxicity, oxidative stress, G2/M arrest, and DNA damage in mouse skin fibroblast cells (L929). Colloids and Surfaces B: Biointerfaces 2015; 125: 73–81. doi: 10.1016/j.colsurfb.2014.11.014
70. Balasubramaniam MP, Murugan P, Chenthamara D, et al. Synthesis of chitosan-ferulic acid conjugated poly (vinyl alcohol) polymer film for an improved wound healing. Materials Today Communications 2020; 25: 101510. doi: 10.1016/j.mtcomm.2020.101510
71. Khandia R, Vishwakarm P, Dhama A, et al. Molybdenum salts possess potent angiogenic modulatory properties: Validation on chorioallantoic membrane (CAM) of chicken. Asian Journal of Animal and Veterinary Advances 2017; 12(1): 44–49. doi: 10.3923/ajava.2017.44.49